Samad, W., Suresh, K., “CAD-Integrated Analysis of 3-D Beams: A Surface-Integration Approach,” Engineering with Computers, vol. 27, no. 3, 201-210, 2011

CAD-Integrated Analysis of 3-D Beams: A Surface-Integration Approach

Wa’el Abdel Samad, Krishnan Suresh
suresh@engr.wisc.edu
2059, Mechanical Engineering Building
1513 University Avenue
University of Wisconsin, Madison
Madison, WI 53706,
Phone: 608 262 3594 Fax: 608 265 2316

Abstract

Most engineering artifacts are designed *and* analyzed today within a 3-D computer aided design (CAD) environment. However, slender objects such as beams are designed in a 3-D environment, but analyzed using a 1-D beam element, since their 3-D analysis exhibits locking and/or is computationally inefficient. This process is tedious and error-prone.

Here, we propose a *dual-representation* strategy for designing and analyzing 3-D beams, directly from within a 3-D CAD environment. The proposed method exploits classic 1-D beam physics, but is implemented within a 3-D CAD environment by appealing to the divergence theorem. Consequently, the proposed method is numerically and computationally equivalent to classic 1-D beam analysis for uniform cross-section beams. But, more importantly, it matches the accuracy of a full-blown 3-D finite element analysis for non-uniform beams.

1. Introduction

Engineering artifacts are largely designed today within a 3-D computer aided design (CAD) environment for at least 3 reasons: (1) CAD models are unambiguous [1], (2) visualization and manufacturing-planning is easier within a 3-D environment [2], and (3) data exchange of 3-D models is well established[3]. Furthermore, most 3-D components are analyzed via the popular 3-D finite element analysis [4], that is tightly integrated with CAD systems today.

However, high-aspect ratio beams pose unique challenges to 3-D FEA. Specifically, consider the beam problem in Figure 1a. If one uses a coarse finite element mesh (element size>>thickness) as in Figure 1b, the presence of poor-quality elements lead to *Poisson locking* [5].

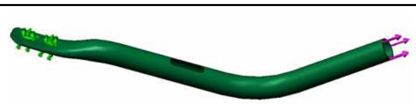

(a) A 3-D beam problem

(b) A coarse mesh.

(c) A fine mesh.

Figure 1: Finite element analysis of a 3-D beam.

On the other hand, if a high quality mesh (element size ~ thickness) is used, the computational cost grows rapidly with the aspect ratio as illustrated in Figure 2 (aspect ratio is the overall length divided by the thickness of the hollow beam).

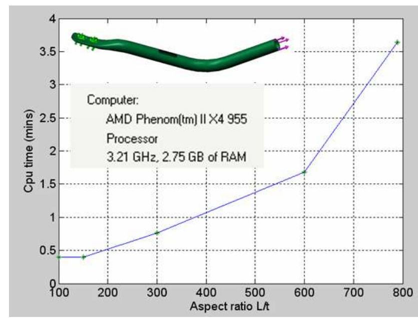

Figure 2: 3-D FEA cpu-time vs. aspect-ratio of a beam, for a high-quality mesh.

Thus thin beams must typically be analyzed using a 1-D beam element, using classic dimensional reduction. Specifically, given a 3-D beam such as the one in Figure 3a, the analyst must create a 1-D beam-element, and assign the appropriate cross-sectional properties as in Figure 3b. The 3-D surface tractions are also translated into equivalent 1-D forces and moments, and finally the 1-D beam problem is solved via 1-D beam analysis.

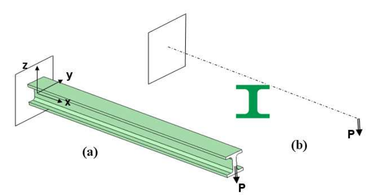

Figure 3: (a) A uniform cross-section beam, (b) 1-D classic dimensional reduction.

The data-transfer between the 3-D CAD environment and 1-D analysis environment is cumbersome and error-prone. For example, consider the beam in Figure 4; extracting its cross-sectional properties is non-trivial, and so is the transfer of the traction forces. Finally, once the 1-D beam is analyzed and optimized, the 3-D CAD model must be reconstructed to reflect the design changes.

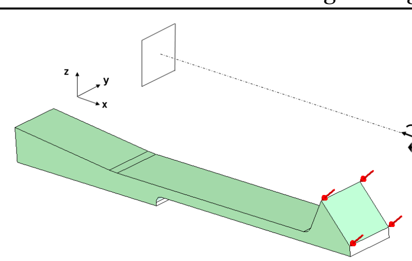

Figure 4: Traction forces on a cantilevered beam.

Indeed, it is well recognized today that direct 3-D CAD-based analysis is highly desirable [6]. Amongst the various 3-D analysis techniques that are known today, the most ‘obvious’ choice is 3-D finite element analysis (FEA). However, as mentioned earlier [5], 3-D FEA of thin structures leads to a locking phenomena and is computationally unattractive.

Alternate and specialized 3-D analysis techniques have been proposed for analyzing thin structures. One such method is based on the concept of solid-shell elements where relatively low order shape functions are used across the thickness to overcome ill-conditioning, etc. However, solid-shell elements entail a priori orientation of the finite element mesh [7]; this can pose difficulties during mesh generation. Reduced integration techniques have also been proposed by several researchers to suppress the deficiencies of standard 3-D FEA [8, 9]. However, under-integration causes generation of hourglass modes and needs stabilization. Alternately, one can exploit hybrid or mixed formulations [6], where both displacements and stresses are treated as free variables. These hybrid elements typically exhibit higher accuracy than regular elements when modeling 3-D thin structures [6]. There are however two challenges: (1) the computational cost of hybrid formulation is significant, and (2) the accuracy does not match the accuracy of classic 2-D mid-surface analysis. More recently, an algebraic-reduction method was proposed in [10] for CAD-integrated analysis of beams. However, algebraic reduction entails specialized assembly procedures, and computationally more expensive than classic 1-D beam analysis.

Given these limitations, we propose here a *dual-representation* method for analyzing 3-D beams. The proposed method exploits classic 1-D beam physics, but is implemented within a 3-D CAD environment by appealing to the divergence theorem. Since the physics is represented in 1-D and the geometry co-exists in 3-D, the proposed method is referred to as a dual-representation method.

The paper is organized as follows. In Section 2, classic beam theory for uniform cross-section beams is briefly reviewed, followed by typical 1-D methods employed today for analyzing non-uniform cross-section beams. Then, in Section 3, the dual representation method is described for static and modal analysis of non-uniform cross-section beams via Euler-Bernoulli and Timoshenko theories. This is followed by numerical experiments in Section 4, where we show that the proposed method matches the automation of 3-D FEA for complex beams, while it matches the accuracy of 1-D analysis. In Section 6, we conclude with open issues and future work.

For the remainder of the paper, beams are assumed to be oriented along x direction, and the bending direction is assumed to be along z, as illustrated in Figure 3.

2. Analysis of Beams: Brief Review

We now briefly review well-established 1-D beam analysis methods (classic dimensional reduction). The review serves as a foundation for the proposed method.

Consider the uniform cross-section beam illustrated in Figure 3a. In the Euler-Bernoulli formulation, it is assumed that the plane normal to the neutral axis remains planar, and perpendicular to the neutral axis [11, 12]. Mathematically, this implies that the 3-D displacements can be expressed as:

$$\begin{aligned} u(x,y,z) &\approx -z w_{0,x} \\ w(x,y,z) &\approx w_0(x) \end{aligned} \tag{2.1}$$

where $w_0(x)$ is a 1-D function defined over the 1-D beam axis; typically, $w_0(x)$ is approximated via Hermite functions $H_i(x)$ [12]:

$$w_0(x) = \left\{ H_1(x) \quad H_2(x) \quad H_3(x) \quad H_4(x) \right\} \hat{w}_0 \tag{2.2}$$

By considering the axial strain energy $\varepsilon_{xx}\sigma_{xx}$, one can show that the components of the Euler-Bernoulli stiffness matrix are given by [11, 12]:

$$K_{ij} = \int_{\Omega} E z^2 H_{i,xx}(x) H_{j,xx}(x) d\Omega; \quad i,j = 1..4 \tag{2.3}$$

Observe that the integral is over the 3-D beam Ω (a trivial but important observation). To reduce the integration to 1-D, one can appeal to the fact that Ω can be expressed as $[0,l] \otimes A$, where A is the cross-sectional area, resulting in:

$$K_{ij} = \int_0^l \int_A E z^2 H_{i,xx}(x) H_{j,xx}(x) dA\, dx \tag{2.4}$$

Integrating over z, we have:

$$K_{ij} = \int_0^l E I H_{i,xx}(x) H_{j,xx}(x) dx \tag{2.5}$$

where:

$$I = \int_A z^2 dA \tag{2.6}$$

Further, one can symbolically integrate Equation (2.5) over x to get a closed-form expression for K_{ij} [12].

Consider now the non-uniform beam in Figure 4. Since the cross-section $A(x)$ is a function of x, K_{ij} is given by:

$$K_{ij} = \int_0^l \int_{A(x)} E z^2 H_{i,xx}(x) H_{j,xx}(x) dA\, dx \tag{2.7}$$

If $A(x)$ is sufficiently simple, Equation (2.7) can evaluated analytically. For example, tapered Timoshenko beams are addressed in [13]. Filleted beams are considered in [14] where lumped-parameter are developed as an addition to the uniform beam model. For multi-stepped beams, the composite element method is proposed in [15] where the beam can be treated as a uniform beam from a finite element perspective. While these address very specific beam configurations, extraction of beam properties requires extensive CAD programming, and is challenging. We show next, how one can avoid case-by-case analysis by integrating the above shape functions over the boundary of the CAD model, and therefore does not entail extraction of cross-sectional properties.

3. Dual-Representation Analysis

As mentioned earlier, in the proposed method, the physics is captured in 1-D beam physics, but the geometry is retained in 3-D.

3.1 Stiffness Matrix for Symmetric Beams

Consider again Equation (2.3), i.e.,

$$K_{ij} = \int_{\Omega} E z^2 H_{i,xx}(x) H_{j,xx}(x) d\Omega \tag{2.8}$$

Since the integral is over the 3-D beam Ω, instead of proceeding to Equation (2.7), let us recall the divergence theorem that states that for any differentiable vector function $\vec{F}$ [16]:

$$\int_{\Omega} \nabla \cdot \vec{F} d\Omega = \int_{\partial\Omega} \vec{F} \cdot \vec{n} d\Gamma \tag{2.9}$$

where $\vec{n}$ is the boundary normal, and $\partial\Omega$ is the boundary of Ω. We now seek $\vec{F}$ such that $\nabla \cdot \vec{F}$ is exactly equal to the integrand in Equation (2.8). Various possibilities exist; for example:

$$\vec{F} = \frac{Ez^3}{3} H_{i,xx}(x) H_{j,xx}(x) \hat{k} \tag{2.10}$$

Thus:

$$\nabla \cdot \vec{F} = \frac{\partial}{\partial z}\left[\frac{Ez^3}{3} H_{i,xx}(x) H_{j,xx}(x)\right] \tag{2.11}$$

i.e.,

$$\nabla \cdot \vec{F} = E z^2 H_{i,xx}(x) H_{j,xx}(x) \tag{2.12}$$

From Equations (2.9) and (2.10):

$$\int_{\Omega} \nabla \cdot \vec{F} d\Omega = \int_{\partial\Omega} \frac{Ez^3}{3} H_{i,xx}(x) H_{j,xx}(x) n_z d\Gamma \tag{2.13}$$

Thus:

$$K_{ij} = \int_{\partial\Omega} \frac{Ez^3}{3} H_{i,xx}(x) H_{j,xx}(x) n_z d\Gamma \tag{2.14}$$

where n_z is z-component of boundary normal. Thus, one can compute the stiffness matrix via Equation (2.14) through simple boundary integration. Note that portion of the boundary where $n_z \neq 0$ needs to be considered.

On the other hand, suppose:

$$\vec{F} = E z^2 G_{ij}(x) \hat{i} \tag{2.15}$$

where $G_{ij}(x)$ is defined via the indefinite integral:

$$G_{ij} = \int_{\partial\Omega} H_{i,xx}(x) H_{j,xx}(x) dx \tag{2.16}$$

then it is easy to show that:

$$K_{ij} = \int_{\partial\Omega} E z^2 G_{ij}(x) n_x d\Gamma \tag{2.17}$$

Observe that $G_{ij}(x)$ in Equation (2.16) is computed once, and is independent of the beam geometry. Now only portion of the boundary where $n_x \neq 0$ needs to be considered.

From the derivation it is easy to show that Equations (2.7), (2.14) and (2.17) are equivalent. In other words, boundary integration results in exactly the same stiffness matrix as in classic 1-D beam analysis. The implementation details are considered later on.

3.3 Asymmetric Beams

For asymmetric beams such as the one in Figure 4, the kinematics needs to be generalized from Equation (2.1) to:

$$\begin{aligned} u(x,y,z) &\approx u_0(x) - z w_{0,x} \\ w(x,y,z) &\approx w_0(x) \end{aligned} \tag{2.18}$$

where $u_0(x)\,\&\,w_0(x)$ are the axial and bending displacements. The unknown displacements $u_0(x)$ and $w_0(x)$ are typically approximated via:

$$\begin{aligned} u_0(x) &= N^u \hat{d}_0 \\ w_0(x) &= N^w \hat{d}_0 \end{aligned} \tag{2.19}$$

where:

$$\begin{aligned} N_u &= \left\{Q_1(x) \quad 0 \quad 0 \quad Q_2(x) \quad Q_3(x) \quad 0 \quad 0\right\} \\ N_w &= \left\{0 \quad H_1(x) \quad H_2(x) \quad 0 \quad 0 \quad H_3(x) \quad H_4(x)\right\} \end{aligned} \tag{2.20}$$

where Q_i are quadratic shape function, and $\hat{d}_0$ are the 7 degrees of freedom include 3 for axial stretching, and 4 for bending:

$$\hat{d}_0 = \left\{\hat{u}_1 \quad \hat{w}_1 \quad \hat{\theta}_1 \quad \hat{u}_2 \quad \hat{u}_3 \quad \hat{w}_2 \quad \hat{\theta}_2\right\} \tag{2.21}$$

Observe that the beam stress is given by:

$$\sigma_{xx} = E\left(u_{0,x} - z w_{0,xx}\right) \tag{2.22}$$

Further, it is easy to show that the stiffness matrix is given by:

$$K_{ij} = \int_{\Omega} E\left[\left(N^u_{i,x} - z N^w_{i,xx}\right)\left(N^u_{j,x} - z N^w_{j,xx}\right)\right] d\Omega \tag{2.23}$$

i.e.,

$$K_{ij} = \int_{\Omega} E \begin{bmatrix} N^u_{i,x} N^u_{j,x} - z\left(N^w_{i,xx} N^u_{j,x} + N^u_{i,x} N^w_{j,xx}\right) \\ + z^2 N^w_{i,xx} N^w_{j,xx} \end{bmatrix} d\Omega \tag{2.24}$$

Reducing the integration to the boundary results in:

$$K_{ij} = \int_{\partial\Omega} E \begin{bmatrix} z N^u_{i,x} N^u_{j,x} \\ -\dfrac{z^2}{2}\left(N^w_{i,xx} N^u_{j,x} + N^u_{i,x} N^w_{j,xx}\right) \\ +\dfrac{z^3}{3} N^w_{i,xx} N^w_{j,xx} \end{bmatrix} n_z d\Gamma \tag{2.25}$$

Again, only the portion of the boundary where $n_z \neq 0$ needs to be considered; these are identified in Figure 5.

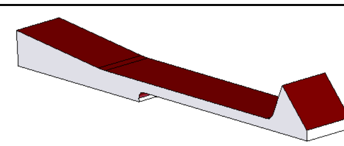

Figure 5: Faces with $n_z \neq 0$ highlighted.

If the equivalent of Equation (2.17) is adopted, then the boundary faces identified in Figure 6 where $n_x \neq 0$ are used. For simplicity, we shall adopt Equation (2.25) for the rest of the paper.

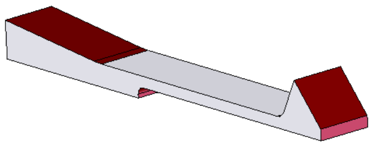

Figure 6: Faces with $n_x \neq 0$ highlighted.

3.2 Boundary Integration Techniques

Almost all CAD systems today can generate a surface triangulation of a solid model rapidly. This is ideal for computing the stiffness matrix since the quality of the triangulation is not relevant for the boundary integration. In particular, given a triangulation of $\partial\Omega$, Equations (2.14) reduces to the form:

$$K_{ij} = \sum_{T_k \subset \partial\Omega} \int_{T_k} \begin{bmatrix} zN^u_{i,x}N^u_{j,x} \\ \dots \end{bmatrix} n_z d\Gamma \tag{2.26}$$

Now, to evaluate the integral over each triangle, one can exploit the algorithms described in [17] or perform Gaussian integration. Only the triangles highlighted in Figure 7 need to be considered.

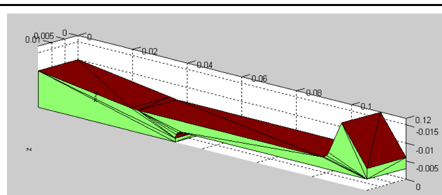

Figure 7: Triangles with $n_z \neq 0$.

Thus far, it was assumed that a single beam-element is used to model the entire 3-D beam structure. Consequently, further division of the triangles was not necessary.

Typically, multiple beam-elements are necessary to capture the physics; for example, Figure 8 illustrates the use 2 beam-elements to capture the sudden change in cross-section. (In reality, the virtual 1-D beam discretization is automated, and happens 'behind-the-scene').

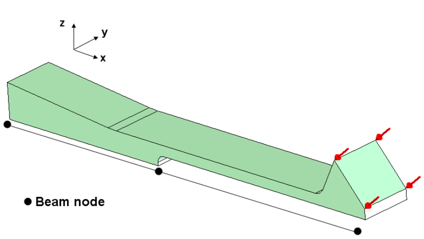

Figure 8: Modeling via 2 beam-elements

This implies that, given a triangulation of the beam, one must split it at the juncture. This is fairly straight-forward to implement as illustrated in Figure 9. In Figure 9a, we start with an initial triangulation consisting of 3 triangles. Now, suppose we wish to integrate over a portion as illustrated in Figure 9b, then, the triangles are split as shown in Figure 9c, and the integration is carried out.

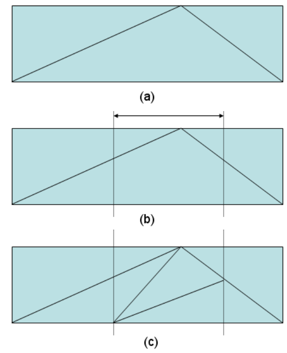

Figure 9: (a) Triangulation, (b) desired integration over sub-region, (c) triangulation of the sub-region.

For the 2 beam-element illustrated in Figure 9a, the resulting triangulation is illustrated in Figure 10

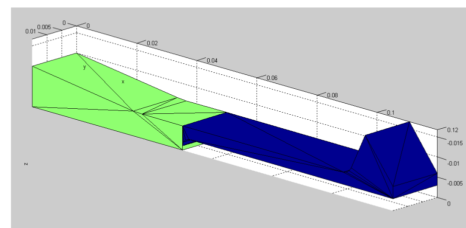

Figure 10: Splitting of a triangulation for 2 beam-elements.

3.4 Traction Forces for Asymmetric Beams

The force contributions are also fairly straightforward to compute. For example, consider the tractions in Figure 4; we shall assume that these tractions are prescribed as $t_x(x,z)$ and $t_z(x,z)$ components over the boundary. The virtual work is therefore given by:

$$\delta W = \int_{\Gamma_N} [\delta u t_x + \delta w t_z] d\Gamma \tag{2.27}$$

Exploiting the definitions in Equation (2.18) and the shape functions in Equation (2.19), the force contributions are:

$$f = \int_{\Gamma_N} \left[\left(N^u - zN^w_{,x} \right) t_x + N^w t_z \right] d\Gamma \tag{2.28}$$

Finally, one can evaluate Equation (2.28) on a surface triangulation via the algorithms described in [17]. Thus, the various 1-D beam loads and moments are determined in a systematic fashion.

3.5 Mass Matrix for Asymmetric Beams

The mass matrix derivation follows a similar process. For example, if one considers an asymmetric beam via the Euler-Bernoulli formulation, the mass matrix components are given by [12]:

$$M_{ij} = \int_{\Omega} \rho \left[\left(N^u_i - zN^w_{i,x} \right) \left(N^u_j - zN^w_{j,x} \right) + N^w_i N^w_j \right] d\Omega \tag{2.29}$$

i.e.,

$$M_{ij} = \int_{\Omega} \rho \begin{bmatrix} N_i^u N_j^u + N_i^w N_j^w \\ -z\left(N_{i,x}^w N_j^u + N_i^u N_{j,x}^w\right) \\ +z^2\left(N_{i,x}^w N_{j,x}^w\right) \end{bmatrix} d\Omega \tag{2.30}$$

Applying the divergence theorem results in:

$$M_{ij} = \int_{\partial\Omega} \rho \begin{bmatrix} z\left(N_i^u N_j^u + N_i^w N_j^w\right) \\ -\dfrac{z^2}{2}\left(N_{i,x}^w N_j^u + N_i^u N_{j,x}^w\right) \\ +\dfrac{z^3}{3}\left(N_{i,x}^w N_{j,x}^w\right) \end{bmatrix} n_z d\Gamma \tag{2.31}$$

The above boundary integration is then evaluated over the triangulation as described earlier.

3.6 Timoshenko Beams

For shear-deformable beam theories such as Timoshenko beam theory, instead of Equation (2.18), we have:

$$\begin{aligned} u(x,z) &\approx u_0(x) + z\theta_0(x) \\ w(x,z) &\approx w_0(x) \end{aligned} \tag{2.32}$$

Further, to avoid locking, one can use, for example, the shape functions associated with the T2CL6 element described in [18], instead of the shape functions in Equation (2.20). Besides these two changes, the rest of derivation is identical to Euler-Bernoulli formulation. As an illustration, please see Appendix A for a derivation of the stiffness matrix.

4. Numerical Experiments

We present here results from a variety of numerical experiments. In all experiments, we assume the following unless otherwise specified:

$$\begin{aligned} E &= 2e^{11} N/m^2 \\ \upsilon &= 0.33 \\ \rho &= 8000 kg/m^3 \end{aligned} \tag{2.33}$$

We compare our results against analytical results if available; else, we use a very high quality 3-D finite element analysis for comparison. Section 4.1 focuses on static problems, while Section 4.2 focuses on modal problems.

4.1 Static Problems

4.1.1 Rectangular Cross-Section Beam

The first verification experiment is the static analysis of a thin rectangular cross-section beam, of length L=1m (along x), width (along y) of 0.1m, and height (along z) as specified in Table 1. The beam is fixed at x=0, and is subject to a z-tip force of 1 N at x = L. The numerical results are presented below in Table 1. Observe that there is no locking in that there is no loss in accuracy as the aspect ratio increases.

Table 1: Static deflection of a rectangular cross-section beam.

	Analytical Results $\frac{PL^3}{3EI}$	Dual-Rep Euler-Bernoulli (7 dof)
h = 0.05m	$6.0e^{-8}$	$6.0e^{-8}$
h = 0.01m	$7.5e^{-6}$	$7.5e^{-6}$
h = 0.001m	0.0075	0.0075

4.1.2 Slotted I-Beam

The real advantage of the proposed method is in modeling non-uniform cross-section, beams. For example, consider the I-beam in Figure 11 that has a pair of slots as illustrated. The total length of the I-beam is 5m; the slots are centered on the I-beam, and have a total length of 1 m, a width of 50 mm (marked 'd'), and are at a distance of 10 mm from the sides, as illustrated.

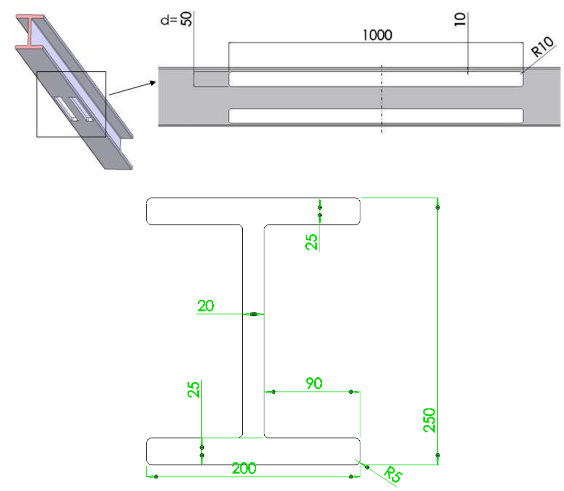

Figure 11: An I-beam with slotted feature.

The objective is to compute the maximum deflection of the I-beam, as the slot-width, denoted by 'd', is varied. In classic 1-D analysis, one must explicitly compute cross-sectional properties across the slotted section, and import that into the 1-D model. Here, we extract the triangulation of the 3-D CAD model, and compute the stiffness matrix via the Timoshenko beam-model with 10 beam elements (63 dof). We use the commercially available COSMOSWorks FEA [19] (with about 133,000 dof) for comparison. The numerical results are tabulated in Table 2; typical CPU time taken is also tabulated.

Table 2: Static deflection of a slotted I-beam (meters).

	3-D FEA (~133,000 dof)	Dual-Rep Timoshenko (63 dof))
$d = 20mm$	$1.324e^{-8}$	$1.322e^{-8}$
$d = 50mm$	$1.400e^{-8}$	$1.391e^{-8}$
$d = 70mm$	$1.491e^{-8}$	$1.476e^{-8}$
CPU time	*83 seconds*	*0.7 seconds*

Observe that, the predicted deflection is within 1% of the 3-D solution, while the computational cost is 2 orders of magnitude smaller.

Samad, W., Suresh, K., "CAD-Integrated Analysis of 3-D Beams: A Surface-Integration Approach," Engineering with Computers, vol. 27, no. 3, 201-210, 2011

Since the analysis is carried out using a 3-D CAD model, one can, for example, compute and display the 3-D displacements via Equation (2.18). However, while a coarse triangulation is sufficient for accurate prediction of deflections and stresses, a finer triangulation is desirable (purely) for visualization. Figure 12 illustrates the deformation of the 3-D beam, as predicted via the proposed method.

Further, one can extract the beam stresses via Equation (2.22); this is illustrated in Figure 12. As can be observed in Figure 12, the proposed method accounts for the reduced cross-section near the slot (the stresses are accurate to within 3% of the 3-D nominal stress). One cannot however capture the 3-D stress concentrations via beam physics; this entails sub-modeling [20], and is not pursued in this paper.

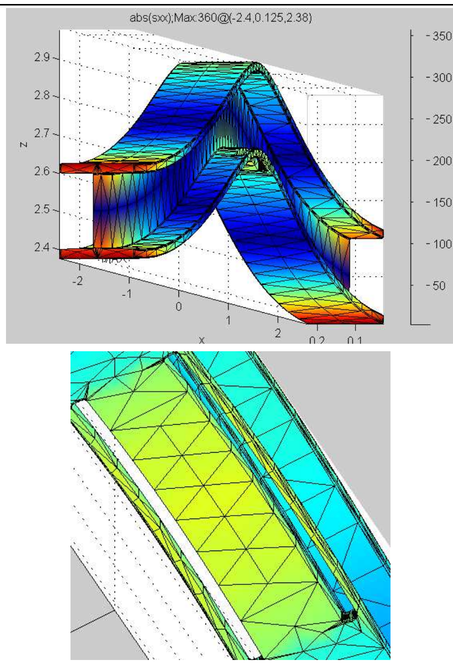

Figure 12: Beam stress $|\sigma_{xx}|$ over slotted I-beam.

4.1.3 A Stiffened Structure

Consider next the static deflection of a beam-like structure illustrated in Figure 13. Such structures are analyzed today by decomposing them into numerous beam elements, and computing the cross-sectional properties of each beam. However, in the proposed method, one can use a single (virtual) beam as illustrated, and use boundary integration to carry out an equivalent beam-analysis.

Indeed, a 3-D FEA (with 80,000 dof) predicts a deflection of 0.221 mm, while the proposed method (with 50 dof) predicts a deflection of 0.215 mm. Thus, with judicious approximation, one can attain considerable computational speed-ups, with minimal loss in accuracy.

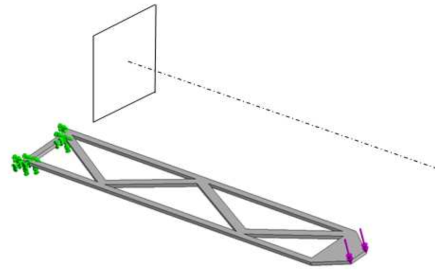

Figure 13: A beam-like structure, and 1-D beam.

4.2 Modal Problems

4.2.1 Rectangular Cross-Section Beam

Next, we consider modal problems. The first verification experiment for modal problems is on a rectangular cross-section beam, of length L = 1m (along x), width (along y) of 0.1m, and height (along z) of 0.01m, that is cantilevered at one end. The first few modal values (in Hz) are presented in Table 1 using 20 Euler-Bernoulli elements within the dual-representation framework. Observe that the results closely match the analytical results for an Euler-Bernoulli beam [21].

Table 3: Modes of a rectangular cross-section beam.

	Analytical Results	Dual-Rep Euler-Bernoulli (83 dof)	3-D FEA (20,000 dof)
Mode-1	40.384	40.385	40.552
Mode-2	253.09	253.09	251.19
Mode-3	708.70	708.68	691.06
Mode-4	1388.80	1388.77	1321.76

4.2.2 Filleted Beam

We now study the impact of a fillet on the modes of the above beam; the beam dimensions are identical to the previous example, except that the beam is filleted at the cantilevered end. The radius of the fillet is modified in the experiment below. In current methods of beam analysis, it is difficult to account for the fillet; specialized methods are necessary [14]. In the proposed method, the fillets pose no additional challenge.

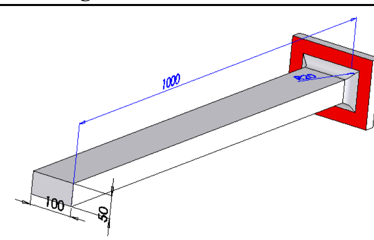

Figure 14: A filleted beam.

The predicted percentage increase in frequencies in the first few modes are presented in the table below for two different radii. As one observe, the proposed method closely matches the 3-D FEA results, at a considerably reduced computational cost.

Table 4: Predicted increase in frequency due to fillets.

		Δf Dual-Rep (EB; 123 dof)	Δf 3-D FEA (25,000 dof)
R = 25 mm	*Mode-1*	+2.0%	+1.7%
	Mode-2	+2.1%	+1.7%
	Mode-3	+2.1%	+1.7%
	Mode-4	+2.0%	+1.6%
R = 50 mm	*Mode-1*	+6.7%	+5.9%
	Mode-2	+6.5%	+5.7%
	Mode-3	+6.4%	+5.5%
	Mode-4	+6.3%	+5.3%

4.2.3 AFM Microcantilever

As a final example, we consider atomic force microscopy (AFM) microcantilevers illustrated in Figure 15 [22]. These cantilevers are beam-like structures with special tips as illustrated. The fundamental frequencies of these AFM tips are critical in many AFM applications [22]. The AFM tip illustrated in Figure 15 has a length of 100 microns, width of 10 microns, and height of 1 micron. The material is silicon (E = 1.124e11, ν = 0.28, ρ = 2330; SI units). The tip has a total height of 25 microns.

In classic beam analysis, the tip mass must be estimated and 'inserted' as a parameter into a 1-D beam model[23]. In the proposed method, the mass contribution is computed in an automated fashion.

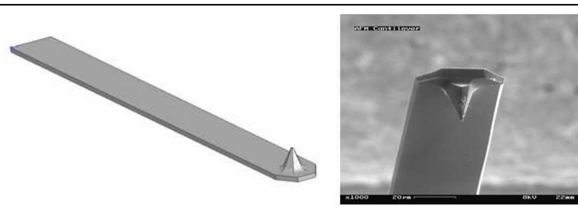

Figure 15: A micro-cantilever

The table below compares the frequencies predicted (in MHz) by the proposed method and 3-D FEA.

Table 5: Modal frequencies (MHz) of a AFM microcantilever.

Frequency In MHz	Dual-Rep Euler-Bernoulli (83 dof)	3-D FEA (14,000 dof)
Mode-1	0.69111	0.69516
Mode-2	4.3839	4.4014
Mode-3	12.387	12.420
Mode-4	24.489	24.455

5. Conclusions

The main contribution of this paper is a CAD-integrated method for computing the static and modal response of geometrically complex 3-D beam-like structures. For uniform cross-section beams, the proposed method is equivalent to classic 1-D beam theory. For more complex beams, the results closely match 3-D FEA results, with far fewer degrees of freedom.

Future work will focus on: (1) coupling of 3-D finite element analysis (over non-slender regions of complex geometries) with implicit 1-D beam analysis (over slender regions), and (2) computing, in a posteriori sense, the modeling error due to possibly incorrect 1-D beam assumptions.

Appendix A: Boundary Integration for the Timoshenko Beam

In Timoshenko beam theory, the displacements are approximated via Equation (2.32), where $u_0(x)$, $w_0(x)$ and $\theta_0(x)$ are the axial, bending and rotation of a transverse normal about the y-axis. To avoid locking, we use the shape functions associated with the T2CL6 Timoshenko beam element described in [18]. This beam element (see Figure 16) has a total of 10 degrees of freedom with one degree of freedom w_α that is eliminated.

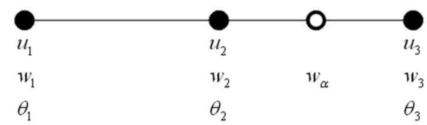

Figure 16: The T2CL6 beam element.

The unknown functions $u_0(x)$, $w_0(x)$, and $\theta_0(x)$ are approximated in this beam element via:

$$u_0(x) = N^u \hat{d}_0$$
$$w_0(x) = N^w \hat{d}_0$$
$$\theta_0(x) = N^\theta \hat{d}_0$$

where:

$$N^u = \begin{Bmatrix} (\xi^2-\xi)/2 \\ 0 \\ 0 \\ (-\xi^2+1)/2 \\ 0 \\ 0 \\ (\xi^2+\xi)/2 \\ 0 \\ 0 \end{Bmatrix}^T ; N^\theta = \begin{Bmatrix} 0 \\ 0 \\ (\xi^2-\xi)/2 \\ 0 \\ 0 \\ (-\xi^2+1)/2 \\ 0 \\ 0 \\ (\xi^2+\xi)/2 \end{Bmatrix}^T ;$$

are the usual quadratic shape-functions while the shape function for the $w_0(x)$:

$$N^{w} = \begin{Bmatrix} 0 \\ (\xi^2-\xi)/2 \\ L(\xi^3-\xi)/12 \\ 0 \\ (-\xi^2+1)/2 \\ L(-\xi^3+\xi)/6 \\ 0 \\ (\xi^2+\xi)/2 \\ L(\xi^3-\xi)/12 \end{Bmatrix}^{T}$$

is obtained by applying the constraint discussed in [18] to avoid locking. Notice that $w_0(x)$ is approximated via a polynomial that is one order higher than $\theta_0(x)$.

Further, the beam stresses are given by:

$$\begin{aligned} \sigma_{xx} &= E\left(u_{0,x} + z\theta_{0,x}\right) \\ \sigma_{xz} &= kG\left(\theta_0 + w_{0,x}\right) \end{aligned}$$

where k and G are the shear correction factor and shear modulus respectively. Accounting for the axial and shear strain energies, it is easy to show that the stiffness matrix is now given by:

$$K_{ij} = \int_{\Omega} \begin{bmatrix} E\left(N^{u}_{i,x} + zN^{\theta}_{i,x}\right)\left(N^{u}_{j,x} + zN^{\theta}_{j,x}\right) + \\ kG\left(N^{\theta}_{i} + N^{w}_{i,x}\right)\left(N^{\theta}_{j} + N^{w}_{j,x}\right) \end{bmatrix} d\Omega$$

i.e.,

$$K_{ij} = \int_{\Omega} \begin{Bmatrix} E\begin{bmatrix} N^{u}_{i,x}N^{u}_{j,x} + z\left(N^{u}_{i,x}N^{\theta}_{j,x} + N^{\theta}_{i,x}N^{u}_{j,x}\right) \\ +z^2 N^{\theta}_{i,x}N^{\theta}_{j,x} \end{bmatrix} + \\ kG\left[N^{\theta}_{i}N^{\theta}_{j} + N^{\theta}_{i}N^{w}_{j,x} + N^{w}_{i,x}N^{\theta}_{j} + N^{w}_{i,x}N^{w}_{j,x}\right] \end{Bmatrix} d\Omega$$

Reducing the integration to the boundary results in the boundary form of the Timoshenko T2CL6 stiffness matrix:

$$K_{ij} = \int_{\partial\Omega} \begin{Bmatrix} E\begin{bmatrix} zN^{u}_{i,x}N^{u}_{j,x} + \dfrac{z^2}{2}\left(N^{u}_{i,x}N^{\theta}_{j,x} + N^{\theta}_{i,x}N^{u}_{j,x}\right) \\ +\dfrac{z^3}{3}N^{\theta}_{i,x}N^{\theta}_{j,x} \end{bmatrix} + \\ kG\begin{bmatrix} zN^{\theta}_{i}N^{\theta}_{j} + zN^{\theta}_{i}N^{w}_{j,x} + \\ zN^{w}_{i,x}N^{\theta}_{j} + zN^{w}_{i,x}N^{w}_{j,x} \end{bmatrix} \end{Bmatrix} n_z d\Gamma$$

Acknowledgements

The authors wish to acknowledge the support of the National Science Foundation under grants OCI-0636206, and CMMI-0726635, CMMI-0745398.

References

1. Requicha, A.G., *Representations for Rigid Solids: Theory, Methods, and Systems*. ACM Computing Surveys (CSUR), 1980. **12**(4): p. 437 - 464.
2. Fu M. W., O.S.K., Lu W. F., Lee I. B. H., Nee A. Y. C., *An approach to identify design and manufacturing features from a data exchanged part model*. Computer Aided Design, 2003. **35**: p. 979-993.
3. Pratt M. J., A.B.D., Ranger T., *Towards the standardized exchange of parameterized feature-based CAD models*. Computer Aided Design, 2005. **37**: p. 1251-1265.
4. Zienkiewicz, O.C., Taylor, R. L, Zhu, J. Z., *The Finite Element Method: Its Basis and Fundamentals*. 6th Edition ed. 2005: Elsevier Butterworth Heinemann.
5. Dow, J., Byrd, D. E.,, *The Identification and Elimination of Artificial Stiffening Errors in Finite Elements*. International Journal of Numerical Methods in Engineering, 1988. **26**(3): p. 743-762.
6. Jog, C.S., *A 27-node hybrid brick and a 21-node hybrid wedge element for structural analysis*. Finite Elements in Analysis and Design, 2005. **41**(11-12): p. 1209-1232.
7. Duster, A., Broker, H., Rank E., *The p-Version of Finite Element Method for Three-Dimensional Curved Thin Walled Structures*. International Journal of Numerical Methods in Engineering, 2001. **52**(7): p. 673-703.
8. Braess, D., Kaltenbacher, M., *Efficient 3D-Finite-Element-Formulation for Thin Mechanical and Piezoelectric Structures*. International Journal of Numerical Methods in Engineering, 2007.
9. Dorfmann, A., Nelson, R.B., *Three-Dimensional Finite Element for Analysing Thin Plate/Shell Structures*. International Journal of Numerical Methods in Engineering, 1995. **38**(20): p. 3453-3482.
10. Jorabchi, K., Danczyk, J., Suresh, K., *Algebraic Reduction of Beams for CAD-Integrated Analysis*. CAD, 2008. **Submitted; January 2008**.
11. Wang, C.M., Reddy, J. N., Lee, K. H., *Shear Deformable Beams and Plates: Relationship to Classical Solutions*. 2000, London: Elsevier Science.
12. Pilkey, W., *Analysis and Design of Elastic Beams*. 2002, New York, NY: John Wiley.
13. Zhou, D., Cheung, Y. K., *Vibrations of Tapered Timoshenko Beams in Terms of Static Timoshenko Beam Elements*. Journal of Applied Mechanics, 2001. **68**(4): p. 596 - 603.
14. Lobontiu, N., Garcia, E., *Two Microcantilever Designs: Lumped-Parameter Model for Static and Modal Analysis*. Journal of Microelectromechanical Systems, 2004. **13**(1).
15. Lu, Z.R., Huang, M., Liu, J. K., Chen, W. H., Liao, W. Y., *Vibration analysis of multi-stepped beams with the composite element models*. Journal of Sound and Vibration, 2009. **322**: p. 1070-1080.
16. Bronshtein, I.N., Semendyayev, K. A., *Handbook of Mathematics*. 1985, New York: Van Nostrand Reinhold.
17. Rathod, H.T., Govinda Rao, H. S., *Integration of Trivariate Polynomials over Linear Polyhedra in Euclidean three-dimensional space*. J. Austral. Math. Soc., 1998. **39**: p. 355-385.
18. Tessler, A., Dong, S. B., *On a Hierarchy of Conforming Timoshenko Beam Elements*. Computers and Structures, 1981. **14**(3-4): p. 335-344.
19. SolidWorks, *SolidWorks; www.solidworks.com*. 2005.
20. Zienkiewicz, O.C., Taylor, R. L., *The Finite Element Method for Solid and Structural Mechanics*. 6th ed. 2005: Elsevier.
21. Young, W.C., *Roark's Formulas for Stress and Strain*. 1989, New York: McGraw Hill.

22. Hsu, J.-C., Lee, H-L., Chang, W-J., *Flexural vibration frequency of atomic force microscopy cantilevers using the Timoshenko beam model*. Nanotechnology, 2007. **18**.
23. Akinpelu, F.O., *The Effect of an Attached Mass on an Euler-Bernoulli Beam*. Journal of Engineering and Applied Sciences, 2007: p. 1251-1254.